$$v_{clay} = \frac{(\phi_N - b\phi_D - a_{sd})}{a_{sh} - a_{sd}} \quad (4)$$

Preferably, core analysis has been undertaken and a reliable set of XRD measurements are available to calibrate the calculated v_{clay}, though in the absence of lab data the estimation can be sensibly constrained. However, it is important to recognize the v_{clay} estimation is integral to this workflow, and as such great care should be taken in its estimation.

With a reliable v_{clay} estimation, the bedding-normal elastic stiffness can be calculated for both the bulk rock, as well as the matrix (C_{33} and C_{33m}, respectively). Vernik and Kachanov (2010) showed that a heuristic clay-based model relating bedding-normal velocity ($Vp(0°)$) to shales with 40-45% porosity is compatible with the compaction behavior of shales as effective stress increases. The model assumes the shale has a bimodal composition: (i) the aligned/laminated clay platelets, and (ii) the non-clay component. Thus, the bedding-normal matrix stiffness can be computed using Reuss averaging (Vernik, 2016):

$$Vp(0°) = \sqrt{\frac{C_{33m}(1 - \phi)^{k^*}}{\rho_m(1 - \phi) + \rho_f\phi}} \quad (5)$$

$$C_{33m} = \{v_{clay}/C_{33clay} + (1 - v_{clay})/M_{quartz}\}^{-1}$$

where k^* is an empirical clay-dependent exponent ($k^* = 5.3 - 1.3v_{clay}$), ϕ is total porosity, and ρ_m and ρ_f are the matrix and fluid densities. In shales with porosities less than 40%, empirical models can be used in their place:

$$Vp(0°) = Vp_m(1 - \phi)^k$$
$$Vp_m = 5.69km/s - 3.56v_{clay} + 1.42{v_{clay}}^2 \quad (6)$$
$$k = 2.302 - 0.646v_{clay}$$

When plotted against Vp-Total Porosity (Figure 1), the resulting clay-content estimation from Equation 6 shows a good fit to the rock physics model. Unfortunately, core data was not available for this well, so the model could not be calibrated against absolute values of clay content. Globally, clay content in shales typically ranges between 30-90%, while in the Gulf of Mexico 40-65% is common. Here, a value of ~60% appears to approximate a majority of the interval and is consistent with average shales worldwide (Vernik, 2016). By adjusting Equation 6, and incorporating Rubey and Hubbert's (1959) exponential relationship for porosity and effective stress, the bedding-normal sonic velocity can be calculated for a given vertical effective stress:

$$Vp(0°) = V_{Pm}[1 - \phi_o exp(-\sigma_v'/C_m)]^k \quad (7)$$

where C_m is the inelastic compaction modulus and typically ranges between 24 and 31 MPa (Vernik, 2011) for shales experiencing loading, as opposed to unloading mechanisms (Bowers, 1994). As with Equation 6, this model only applies to shales with porosities ≤40-45%, and thus should not be used in close proximity to mudline where mudrocks are still undergoing rapid compaction. Substituting hydrostatic pressure for pore pressure in Equation 1, results in the normal vertical effective stress, which can be plugged into Equation 7 in place of σ_v'. In this case, Equation 7 becomes a normal compaction trend (NCT). The advantage of this approach is the

resultant NCT varies in accordance with changes in clay-content, unlike typical NCTs that rely on a single exponential fit. A common workaround employed in traditional pressure workflows when the elastic behavior of shales is seen to materially change within a well is to invoke an additional NCT, and often with good reason such as a change in provenance, clay type, or unconformities. However, this approach is not without its limitations, namely the inability to account for variation *within* a contiguous shale, as well as relying on the interpreter to decide when *some* variation becomes *too much* variation for a given NCT.

As a final step in the clay-based pressure prediction workflow, the vertical effective stress is calculated from Equation 7, and inputted into Equation 1 to calculate the pore pressure.

$$\sigma_v' = C_m \ln\left[\phi_0 / \left(1 - (Vp/Vp_m)^{\frac{1}{k}}\right)\right] \quad (8)$$

Results

The workflow described above has been applied to an East Coast Canada well, and the results are shown in Figure 2. Both Equivalent Depth (Vp) and Eaton Ratio (Vp/Resistivity) methods were calibrated to neighboring wells. Pressure measurements (green diamonds) show the sands to be laterally drained and near-normally pressured, as is common for this area (O'Connor et al., 2012). All four methods indicate the shale interval, coloured purple (~x900 to x250m), to be overpressured (~14ppg EMW) and drilled underbalanced. However in the upper 100m of the interval (dark red shaded region), there is a change in the elastic logs, manifested by an increase in Vp & Density, as well as a shift in the neutron log; these changes correspond to an increase in the siltstone fraction as seen in drill cuttings (track 2), and can be observed in the surrounding wells. The traditional methods, using a single NCT, associate this increase in Vp to a decrease in shale porosity, and therefore a marked decrease in pore pressure (~10ppg EMW). The clay-based pressure prediction accounts for the clay-content based on the changes in neutron-density, and produces a prediction (13.5ppg EMW) consistent with the lower portion of the shale interval. Both sets of interpretations imply a shoulder effect to be present at the top of the shale, as would be expected as the overlying sands (shaded light blue) are believed to be normally pressured. Although this example covers a limited depth range, the learnings here can be used to inform casing and mudweight design for subsequent wells.

References

Bowers, G.L. 1994. Pore pressure estimation from velocity data: accounting for overpressure mechanisms besides under-compaction. IADC/SPE Drilling Conference, 27488.

Eaton, B.A. 1975. The equation for geopressure prediction from well logs. Society of Petroleum Engineers 5544.

Foster, J. B. and Whalen, H. E., 1966, Estimation of Formation Pressures From Electrical Surveys-Offshore Louisiana, Journal of Petroleum Technology, 18 (2), pp. 165–171.

O'Connor, S., Green, S., Swarbrick, R., and Lahann, R., 2012, Lateral drainage in the Jeanne d'Arc and Flemish Pass Basins, East Canada [abstract], In: Geoconvention May14-18, 2012, Calgary, Alberta, Canada.

Rubey, W. W., and M. K. Hubbert, 1959, Role of fluid pressure in mechanics of overthrust faulting II: Overthrust belt in geosynclinals area of western Wyoming in light of fluid-pressure hypothesis: Geological Society of America, Bulletin 70, no. 2, 167-206.

Terzaghi, K., 1943, Theoretical Soil Mechanics. New York: John Wiley and Sons.

Vernik, L., 2011, Unified model for continuous pore pressure prediction in shale: 45th US Rock Mechanics/Geomechanics Symposium, American Rock Mechanics Association, conference paper ARMA-11-444.

Vernik, L., 2016, Seismic petrophysics in quantitative interpretation. Society of Exploration Geophysicists.

Vernik, L., and M. Kachanov, 2010, Modeling elastic properties of siliciclastic rocks: Geophysics, 75, no. 6, E171-E182.

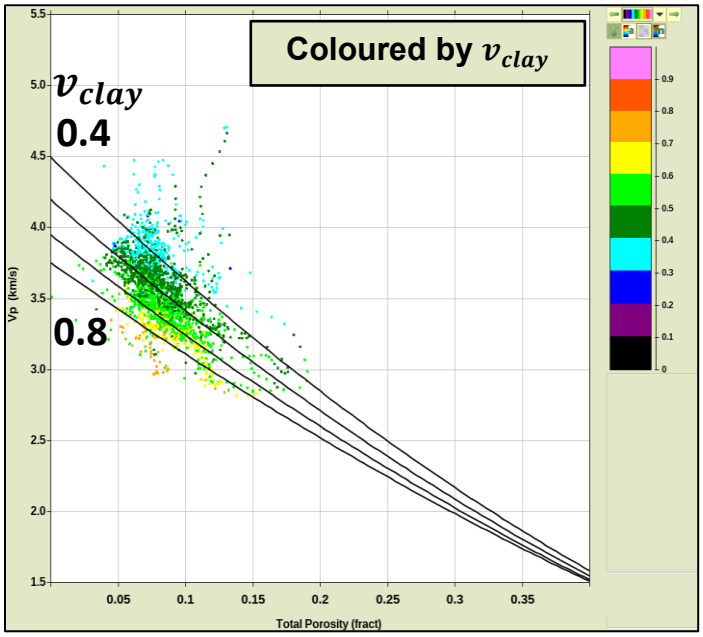

Figure 1 (left): Vp-Total Porosity crossplot, coloured by v_{clay}. Solid lines indicate Vp-total porosity relationships as given by the RPMs in equation 6. A good fit to the RPM shows the v_{clay} calibration from neutron-density to be applicable to this shale.

Figure 2 (below): Log data from an East Coast Canada well. In the Pressure-Depth plot to the right, the clay-based pressure curve (red) is plotted against traditional methods. Dotted lines indicate average pressure gradients from the drill floor in equivalent mudweight (EMW) from 8-20ppg.